Journal of Power Sources 198 (2012) 236–242

Contents lists available at SciVerse ScienceDirect

Journal of Power Sources

journal homepage: www.elsevier.com/locate/jpowsour

# Study of thermal deterioration of lithium-ion secondary cell using an accelerated rate calorimeter (ARC) and AC impedance method

Hiroaki Ishikawa[a,b], Omar Mendoza[a], Yoshitsugu Sone[c], Minoru Umeda[a,*]

[a] Department of Materials Science and Technology, Faculty of Engineering, Nagaoka University of Technology, 1603-1, Kamitomioka, Nagaoka, Niigata 940-2188, Japan
[b] Industrial Technology Institute of Ibaraki Prefecture, 3781-1, Nagaoka, Ibaraki-machi, Higashi-Ibaraki-gun, Ibaraki 311-3195, Japan
[c] Japan Aerospace Exploration Agency, 7-44-1, Jindaiji Higashimachi, Chofu, Tokyo 182-8522, Japan

ARTICLE INFO

*Article history:*
Received 3 August 2011
Received in revised form 4 September 2011
Accepted 21 September 2011
Available online 4 October 2011

*Keywords:*
Lithium-ion secondary cell
Accelerated rate calorimeter
Thermal runaway
Thermal deterioration
Activation-energy
Electrochemical impedance spectroscopy

ABSTRACT

In this study, we analyzed the thermal characteristics of commercial cylindrical lithium-ion cells using an accelerated rate calorimeter (ARC) and by analyzing the electrochemical impedance spectroscopy (EIS) measurements. During the thermal runaway analysis, the cells were tested at different state of charges (SOCs) and the thermal deterioration was determined by monitoring the impedance at 1 kHz and the open circuit voltage as a function of the temperature. The mapping of the thermal runaway was obtained, ant the non-self heating, self-heating and thermal runaway regions were identified at different SOCs. The self-heating and thermal runaway behaviors showed a temperature dependence. In order to clarify the deterioration reaction in the non-self heating region, high temperature storage tests were carried out, storing the cell in the temperature range of 70–100 °C. We estimated the activation energy from the discharge capacities before and after the high temperature storage. In order to determinate the charge/discharge activation energy of the cells, EIS measurements were recorded. Based on our study, the activation energy of the deterioration was about two times greater in magnitude than the activation energy of the charge/discharge.



## 1. Introduction

Lithium-ion secondary cells possess a high energy density, and because of their small size and light weight, these cells have been widely used in portable devices as a power source [1]. In recent years, the use of smaller Li-ion secondary cells in electric, hybrid and plug-in hybrid vehicles have replaced the larger batteries, and a further expansion of their use is expected [2].

During the Li-ion cell charge/discharge, chemical and electrochemical reactions as well as lithium-ions and mass transfer take place, and it is known that many of these reactions are strongly affected by the temperature [3]. Assuming that a vehicle battery is expected to be used under extreme environmental conditions; therefore, it is necessary to control these reactions.

However, extraordinary heating (thermal runaway) is caused by an exothermic reaction that involves the electroactive material, binder and organic solvent when the environmental temperature rises, and the lithium-ion secondary cell is exposed to high temperature conditions [4–7]. In addition, the heat stability of the cells becomes a significant issue because their deterioration is accelerated in the non-heating domain, around 70–100 °C, where the exothermic reaction does not occur [8].

When considering the electric vehicle business, the analysis of the thermal behavior under high temperature conditions as well as the thermal runaway is indispensable from the viewpoint of safety, but the analysis of the deterioration behavior in the non-heating domain is essential from the viewpoint of the battery's lifetime. Therefore, by using an accelerated rate calorimeter (ARC), monitoring the electrochemical and thermal behaviors and observing the open circuit voltage and internal resistance of commercial lithium-ion cells, it was possible to determine the state of charge (SOC) dependence of the self-heating domain and non self-heating domain. In order to analyze in detail the deterioration of the non-heating region for the thermal runaway mapping, discharge capacity measurements were then carried out after storing the cells at comparatively high temperatures. On the other hand, impedance spectroscopy measurements of the lithium-ion secondary cells at elevated temperatures were carried out to determine the activation energy of the charge/discharge, which is determined from the electrochemical parameters using an equivalent circuit. The discharge and deterioration reactions are independent of each other, however, a comparison of these activation energies is an important element in order to understand the thermal deterioration of

* Corresponding author. Tel.: +81 258 47 9323; fax: +81 258 47 9323.
*E-mail address:* mumeda@vos.nagaokaut.ac.jp (M. Umeda).

0378-7753/$ – see front matter © 2011 Elsevier B.V. All rights reserved.
doi:10.1016/j.jpowsour.2011.09.067

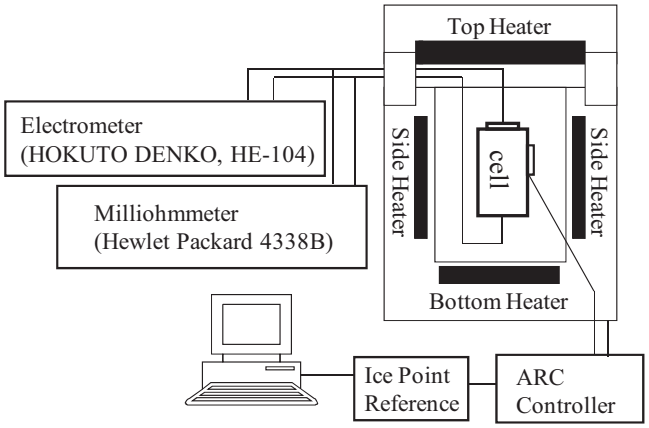


**Fig. 1.** Experimental set up of accelerated rate calorimeter (ARC) for studying thermal runaway characteristics of Li-ion cells.

lithium-ion secondary cells that takes place in the non-heating region.

## 2. Experimental

### 2.1. Cell specifications and SOC adjustment

Thermal runaway examinations using commercial lithium-ion secondary batteries were carried out. Commercially available cylindrical lithium-ion cells (Panasonic CGR18650E) were used with the nominal cell capacity and voltage of 2550 mAh and 3.7 V, respectively. The weight of the cell was 46.5 g and energy density was 520 Wh $l^{-1}$. The cell had a $LiCoO_2$-based cathode, a graphite-based anode [9].

First of all, to determine the cell capacities, charge/discharge tests using a battery charge/discharge equipment were carried out. Based on the results, we determined the SOC of 100%. The cell was charged to the SOC of 100%, and then, discharged to the desired SOC.

### 2.2. Characteristic of thermal runaway process

The thermal runaway experiments were carried out inside an accelerated rate calorimeter (ARC) 2000™ (Colombia Scientific Industries) in combination with a milliohmmeter (Hewlett-Packard, 4338B) and an electrometer (HOKUTO DENKO, HE-104) as shown in Fig. 1. The milliohmmeter measured the resistance at 1 kHz and the electrometer measured the voltage [6].

The cell was placed inside the ARC cavity, being first charged to the desired state of charge (SOC) for at least 12 h, and the cell temperature was measured with a thermocouple attached to the cell surface. The temperature inside the ARC was raised by a method called the Heat-Wait-Search mode using a computer. Fig. 2 shows a conceptual diagram that illustrates the measurements obtained by the Heat-Wait-Search mode. The solid line represents the temperature of the battery surface and the dashed line expresses the temperature inside the ARC. During the heat mode, the interior of the ARC is heating until the target temperature is reached; the heat mode is followed by a wait mode and a search mode. In the wait mode, there is a waiting period until the cell temperature approaches the target value; during the search mode if the heating rate of the cell is greater than 0.05 °C per minute, it is considered an indication of the onset of an exothermic reaction (which is defined as self-heating) [10]. When the self-heating is observed, the ARC shuts down the heating and tracks the cell temperature until the end of the thermal runaway process. The thermal runaway analysis was carried out until the cell surface temperature reached 200 °C.

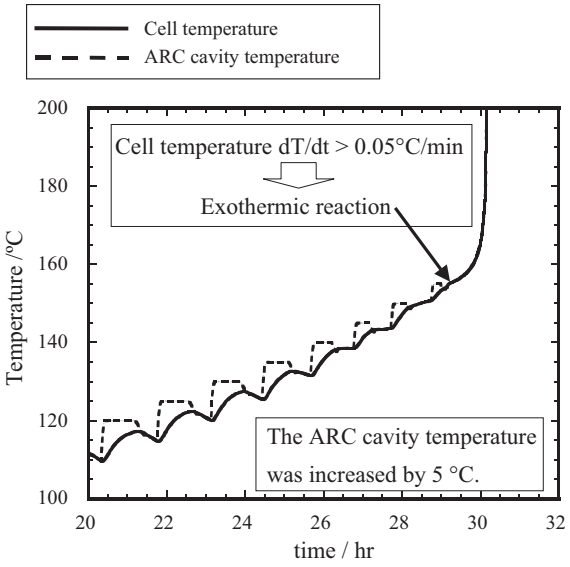


**Fig. 2.** Explanation of Heat-Wait-Search mode in thermal runaway experiments.

In parallel with the mapping of the thermal runaway, the internal resistance and the open circuit voltage were monitored using the milliohmmeter and the electrometer. The internal resistance was obtained by calculating the impedance module $Z$ from expression (1), where $R$ is the resistance component and $X$ is the reactance component.

$$Z = \sqrt{R^2 + X^2} \quad (1)$$

### 2.3. Measurements for calculating activation energy of thermal deterioration

In order to analyze in detail the degradation reactions of the non-self-heating region in the thermal runaway map, the cells were charged to an arbitrary SOC and placed inside a constant temperature chamber (ETAC, HIFREX FL414 PH), and a thermocouple was attached on the cell surfaces to monitor their temperatures. Simultaneously, the voltage of the cells was recorded using a voltmeter (HOKUTO DENKO, HE-104); the measurements were carried out until the voltage fell below 2 V, due to cell failure. Consequently, the time period in which the cell begins to deteriorate (deterioration time) due to high temperature storage was determined.

The cell was kept at the same SOC in the constant temperature chamber, then the cell was taken out before reaching the deterioration time. After that, in order to determine how the cell had degraded, charge/discharge tests using battery charge/discharge equipment (KIKUSUI, PFX2001) were carried out. The charge measurements were recorded under the following conditions: constant current/constant voltage method, 4.2 V maximum voltage, 0.5 C charge current and convergence current of 0.05 C. The discharge measurement conditions were a constant current method, minimum voltage of 2.75 V and discharge current of 0.5 C. C is used to express the nominal capacity. The capacity of the cell tested at high temperature used the second cycle discharge capacity. At the end of the charge or discharge process, a discharge test was carried out at 25 °C; before recording the test, the cell was left inside the temperature chamber for 1 h at 25 °C. The change in capacity was initially calculated, and used as an initial reference before storing the cells and calculating the degradation activation energy.

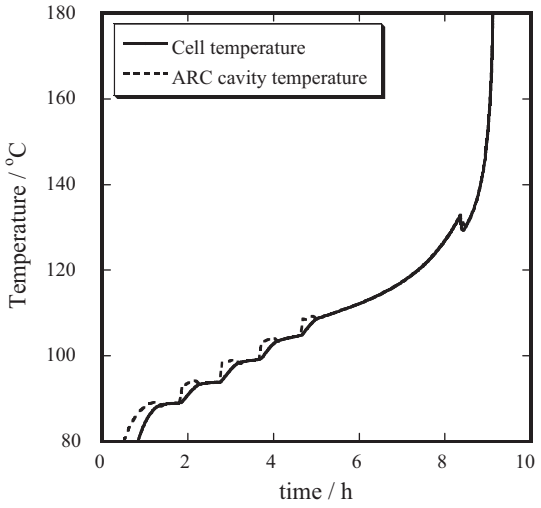


**Fig. 3.** Thermal behavior of cell during thermal runaway experiments at SOC = 87%.

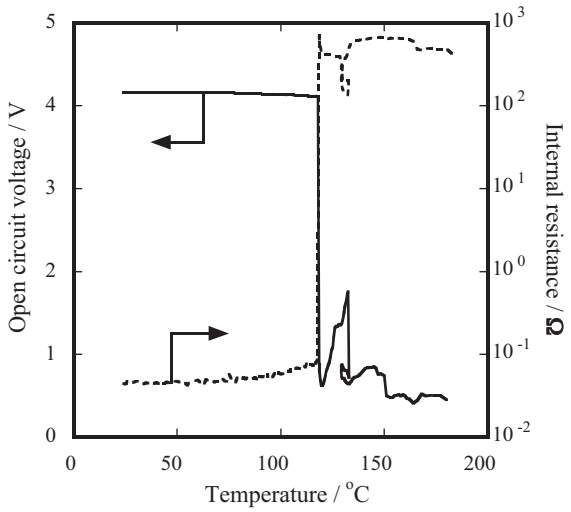


**Fig. 4.** The internal resistance at 1 kHz and the open circuit voltage profile of a cell during thermal runaway experiment as a function of temperature at SOC = 87%.

### *2.4. Measurements for calculating activation energy of charge/discharge reaction*

In order to calculate the activation energy of the charge/discharge reaction, electrochemical impedance spectroscopy (EIS) measurements were recorded. The deterioration and discharge reactions were originally separate, but the discharge reaction was adopted as this was used as a baseline of the deterioration reaction.

Before recording the EIS measurements, the lithium-ion secondary cell, which was initially charged to an arbitrary SOC, was placed inside the temperature chamber (ETAC, HIFREX FL414 PH) and a thermocouple attached to the cell surface. The temperature of the chamber was increased, and the EIS measurements were taken when the chamber reached the set temperature and the surface temperature of the cell was stable. The measurements were carried out using a Li-ion battery analyzing system (NF corporation, As-510-B60) and Servo analyzer (NF corporation, FRA5014), and the AC amplitude and frequency range were 5 mV–rms and 10 kHz to 10 mHz, respectively. The EIS spectra were analyzed using an equivalent circuit, and fitted by ZView software; and then the activation energy of charge/discharge was determined from electrochemical parameters.

## 3. Results and discussion

### *3.1. Mapping of thermal runaway characteristics*

Fig. 3 shows a plot of the cell and ARC cavity temperature changes as a function of the time during the thermal runaway test. As the temperature of cell is higher than the temperature inside the ARC and the self-heating rate is greater than 0.05 °C min$^{-1}$, it can be affirmed that at the temperature of 110 °C, an exothermic reaction takes place, and also the ARC cavity temperature followed the cell temperature, so it was observed that the temperatures of the cell and ARC were the same above 110 °C. A temperature drop occurred at 133 °C. Inside the cell, a gas is generated as a product of the reaction between an electrode and the electrolyte; this gas changed the internal pressure of the cell causing it to explode and the electrolyte exited the cell, which suggested that the temperature drop is due to the heat of vaporization. After leakage of the electrolyte, the cell surface temperature again increased accompanied by a high exothermic reaction that occurred at around 135 °C. The reaction between the solid electrolyte interface (SEI) and the anode and cathode materials has already been reported [11,12].

Fig. 4 shows the plot of the internal resistance and the open circuit voltage as a function of the cell surface temperature. An increase in the internal resistance and a decrease in the open circuit voltage were observed when the temperature increased, and at the temperature of 118 °C, a sudden increase in the internal resistance and decrease in the open circuit voltage were observed. It is believed that a safety mechanism to shut down the cell is activated, and this occurs when the separator of the cell melts [13,14].

Thermal runaway tests were carried out at different SOCs. Fig. 5 shows the non-self heating, self-heating and thermal runaway regions at the different SOCs. The white bar represents the non-self heating domain, the gray is the self-heating and the black is the thermal runaway; (△) indicates the temperature at which the internal resistance increases and the open circuit voltage decreases and (▲) indicates the temperature at which the electrolyte leaks out of the cell. Based on the results, the self-heating and thermal runaway behaviors showed a temperature dependence. It was possible to systematically arrange the non-self heating,

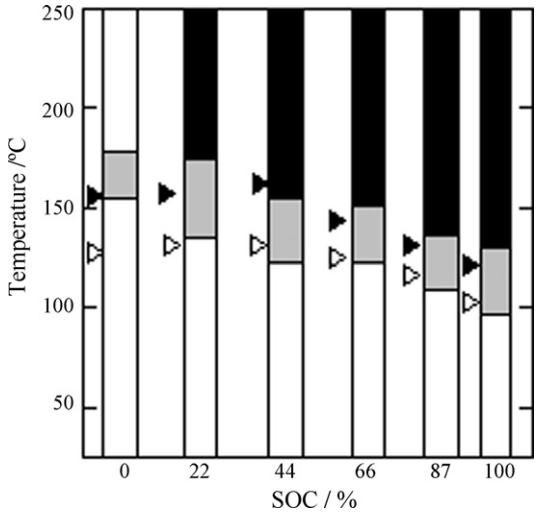


**Fig. 5.** Thermal runaway map. White is non-self-heat area, gray is self-heat area and black is thermal runaway area. (△) indicates the increase in internal resistance and decrease in open circuit voltage. (▲) indicates the electrolyte leakage.

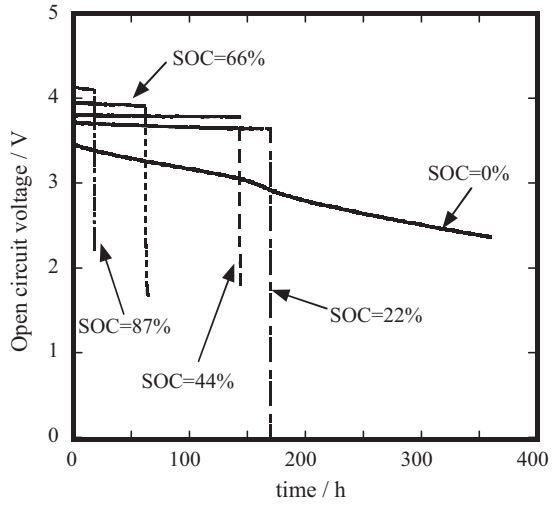


**Fig. 6.** Time dependent open circuit voltage (OCV) change in cell stored at 100 °C.

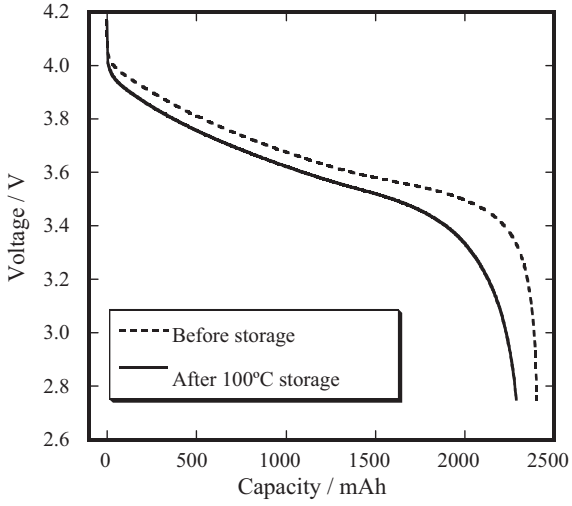


**Fig. 7.** Discharge curves before and after storage test for 7.5 h at SOC = 87%.

self-heating and thermal runaway cell regions by making thermal runaway mapping tests.

### 3.2. The thermal deterioration activation energy

#### 3.2.1. High temperature storage test

The activation energy that causes the cell degradation was calculated by focusing on the non-self heating domain in the thermal runaway map, and analyzing the deterioration reactions that happen in this temperature domain. In order to calculate the deterioration activation energy, high temperature storage tests were carried out at the temperature of 100 °C. Fig. 6 shows the OCV change as a function of the time when the cells were stored at 100 °C. At high temperatures, the OCV slowly decreased, and at the SOC of 87% after 18 h, it was observed that the OCV suddenly decreased. A similar tendency was observed in the cells with the SOC of 22, 44 and 66%, and a suddenly OCV drop was noticed after 18, 62 and 144 h. This sudden OCV drop, considering that 90% of the capacity cell is reduced, is not likely due to the deterioration of the electrodes; rather, it is likely due to the gas that is generated by the reaction between the electrodes and electrolyte because of being exposed for a long time at a high temperature and activates the safety mechanism of the cells due to the increased internal pressure [13]. On the other hand, for the cell with an SOC of 0%, the OCV decrease was slow and no sudden OCV drop was observed. The slow OCV drop is likely due to the irreversible degradation reaction that proceeds in the cell [15]. In addition, we hypothesize that at the SOC of 0%, a sudden OCV drop does not occur, because the electrodes remain stable and only a small quantity of gas is generated.

#### 3.2.2. Calculation of the thermal deterioration activation

Fig. 7 shows a comparison of the discharge curves of the cell at 87% SOC before and after recording the high temperature storage test at 100 °C for 7.5 h. The capacity of the cell was measured after the storage test; the cells were taken out of the temperature chamber before reaching the deterioration point. After the storage test, the cell had a capacity of 2286.5 mAh, while before the storage, the capacity of the cell was 2380.0 mAh, indicating that the capacity of the cell decreased which is shown in Fig. 7. Temperature storage tests were subsequently carried out at 70 °C, 80 °C and 90 °C, and the results are summarized in Table 1. An OCV drop was noticed in all the cases when the cells were stored at high temperatures. From Table 1, it is noted that the deterioration of cells' capacity occurred under all conditions. Therefore, by storing the cells at high temperatures, a type of deterioration is generated.

The reaction rate at the electrode is expressed by (2)

$$v = kc^m \tag{2}$$

where $v$ is the reaction rate, $k$ is the reaction rate constant, $c$ is the lithium-ion concentration, $m$ is the order of reaction. Generally, $m$ is believed to be 1. The relationship between $k$ and activation energy is expressed by the Arrhenius equation as

$$k = k_0 \ \exp\left(\frac{-E_{a1}}{RT}\right) \tag{3}$$

where $k_0$ is the frequency factor, $E_{a1}$ is the deterioration activation energy, $R$ is the gas constant and $T$ is the absolute temperature.

When we define the lithium-ion concentration before and after the degradation as $C_0$ and $C$, respectively, the following expression (4) can be derived from expressions (2) and (3).

$$\ln\frac{C}{C_0} = -k_0 \ \exp\left(\frac{-E_{a1}}{RT}\right) t \tag{4}$$

where $C$ is the electric discharge capacity, $C_0$ is the initial electric discharge capacity, and $t$ is the high temperature storage test time.

Focusing on the activation energy that produces the cell degradation as a method to analyze the behavior of this phenomenon, this can be then obtained using expression (4).

Substituting the values of Table 1 into expression (2) and plotting $\ln[-(\ln C/C_0)/t]$ vs. $1/T$, a straight line is generated. The slope of this line represents the magnitude of the degradation activation energy and the frequency factor is obtained by the intercept of the straight line. Fig. 8 shows a plot that was made from the charge/discharge results after the high temperature storage test at the SOC of 87%. From the line slop, the activation energy that

**Table 1**
Discharge capacity before and after the storage test at SOC = 87% of lithium-ion secondary cells at various temperatures.

| Storage temperature (°C) | Storage time (h) | Capacity (mAh) | | $C/C_0$ |
|---|---|---|---|---|
| | | Before storage ($C_0$) | After storage ($C$) | |
| 70 | 672 | 2429.1 | 2222.4 | 0.915 |
| 80 | 144 | 2423.2 | 2269.1 | 0.936 |
| 90 | 34 | 2425.9 | 2276.2 | 0.938 |
| 100 | 7.5 | 2380.0 | 2286.5 | 0.961 |

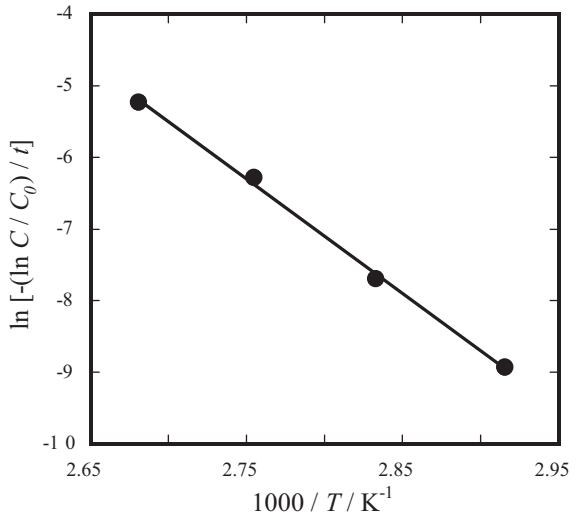


**Fig. 8.** Capacity-deterioration-based Arrhenius plot measured at SOC = 87%. Data are taken from Table 1.

produces deterioration during this period of time is 133.1 kJ mol$^{-1}$. The frequency factor is $6.28 \times 10^{12}$ s$^{-1}$.

Furthermore, following the same method mentioned above, the deterioration activation energy and frequency factor calculations were carried out at SOCs of 0%, 22%, 44%, 66%. These results are summarized in Fig. 9. The lowest values of the activation energy and frequency factor were noted at the SOC of 66%. In other words, the activation energy and frequency factor increase when an unbalance exists between the lithium electrodes, as in the case of the 0% and 87% SOCs, while the minimum deflection was found at the 66% SOC.

As the deterioration reaction progresses very slowly under normal conditions, the data collection would take a long time. Therefore, in order to obtain data about the deterioration reactions in a short period of time, high temperature storage tests and discharge capacity measurement tests were carried out. We think that the deterioration reaction is continuous and the same reaction occurs from normal conditions to 100 °C.

### 3.3. Calculation of the charge/discharge activation energy

Fig. 10 shows the temperature dependence of the impedance measurements at 87% SOC. The impedance measurements were carried out at the different temperatures of 20 °C, 30 °C, 45 °C, and 60 °C. The formation of two semicircles is noted and their size changes with the temperature, i.e., when the temperature increases, the size of the arcs decreases. Therefore, when the temperature increases, the electric resistance decreases. The equivalent circuit shown in the inset of Fig. 10 was used to analyze the obtained impedance spectra. *Rs* expresses the solution resistance in the cell, *R*1 and *CPE*1 represent a resistance component and a constant phase element at high frequency, and *R*2 and *CPE*2 represent a resistance component and a constant phase element at low frequency, respectively. The constant phase element is considered as a non-linear parameter. *Zw* is the Warburg impedance element, which represents the diffusion of the lithium-ions. It is well known that the semicircle at high frequency (*R*1) reflects the anode and the semicircle at low frequency (*R*2) reflects the cathode [16–18].

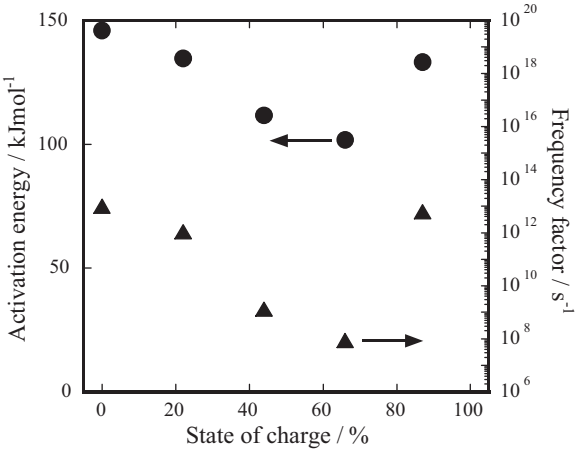


**Fig. 9.** Activation energy of deterioration and frequency factor obtained from lithium-ion secondary cell at various SOCs.

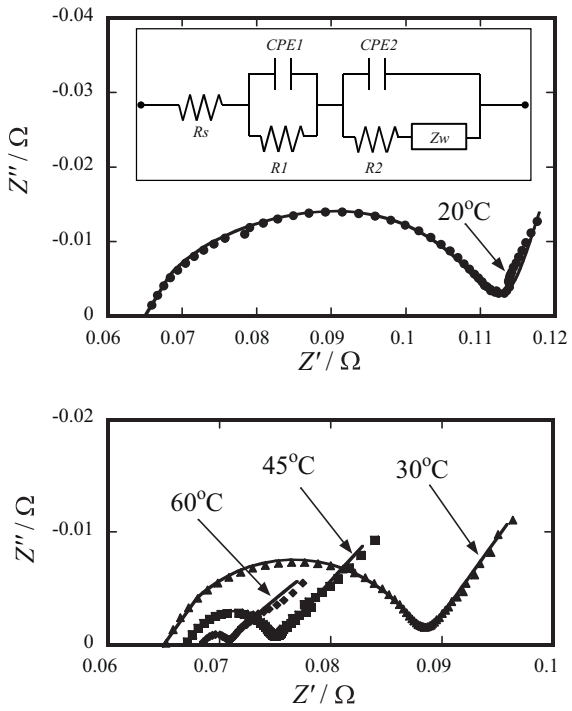


**Fig. 10.** Impedance spectra of lithium-ion secondary cells at SOC = 87%. $Z'$ is real part and $Z''$ is imaginary part of impedance. The upper is measured at 20 °C and lower is measured at 30, 45, and 60 °C. The solid line represents the simulation result. Inset: equivalent circuit used for impedance fitting. *Rs*: ohmic resistance, *R*1 and *R*2: reaction resistance, *CPE*1 and *CPE*2: constant phase element, *Zw*: Warburg impedance.

At the impedance fitting, the precision of the fitting was judged by the chi-squared function ($\chi^2$)[19]. When the $\chi^2$ values in this study were less than $10^{-4}$, we adopt the value. The solid lines represent the simulation results in Fig. 10. Therefore, we confirmed that the equivalent circuit in Fig. 10 is appropriate. The resistance values calculated from Fig. 10 are summarized in Table 2. In this table, by increasing the temperature, the resistance values of *R*1 and *R*2 decreases.

**Table 2**
Resistance components of lithium-ion secondary cell calculated from Fig. 10 at SOC = 87%.

| Temperature (°C) | *Rs* (Ω) | *R*1 (Ω) | *R*2 (Ω) | $\chi^2$ ($\times 10^{-4}$) |
|---|---|---|---|---|
| 20 | 0.065 | 0.019 | 0.026 | 3.7 |
| 30 | 0.065 | 0.010 | 0.013 | 2.5 |
| 45 | 0.067 | 0.004 | 0.004 | 3.3 |
| 60 | 0.068 | 0.001 | 0.001 | 2.2 |

Butler–Volmer equation for charge-transfer controlled electrochemical reaction is given by [20]:

$$R_{ct} = \frac{RT}{nFI_0} \tag{5}$$

where $R_{ct}$ is the reaction resistance, $n$ is the number of the reactive electrons, $F$ is the Faraday constant, $I_0$ is the exchange current of the reaction. From expression (5) and Arrhenius equation, the following expression (6) is derived and $R_{ct}$ could be defined as a function of SOC.

Therefore, the charge/discharge activation energy was then calculated using expression (6) [21].

$$\frac{RT}{nFR_{ct}} = k_0' \exp\left(\frac{-E_{a2}}{RT}\right) \tag{6}$$

where $n$ is the number of the reactive electrons ($n = 1$) and $E_{a2}$ is the charge/discharge activation energy. $k_0'$ of expression (6) is then a fixed number and expressed by Eq. (7).

$$k_0' = FAk_0C^{\alpha} \tag{7}$$

where $A$ is the electrode area, $c$ is the lithium-ion concentration, and $\alpha$ is the transfer coefficient.

The obtained EIS measurements depend of the type of insertion of the lithium-ions, so these are the charge/discharge reactions. Therefore, the charge/discharge activation energy can be calculated by plotting $\ln[RT/nFR_{ct}]$ vs. $1/T$ from expression (4), the value of the slope of the generated straight line represents the charge/discharge activation energy. $R_{ct}$ represents the reaction resistance, so $R_{ct}$ can be substituted by $R1$ and $R2$. In this case, the number of reactive electrons $n$ is 1. Fig. 11 shows the Arrhenius plot of the cell at the SOC of 87%. According to the Arrhenius plot, the charge/discharge activation energy of $R1$ is 54.2 kJ mol$^{-1}$, and the charge/discharge activation energy of $R2$ is 60.9 kJ mol$^{-1}$. This is consistent according to data that has already been reported [21]. In the same way, the charge/discharge activation energy was calculated at the different SOCs. These results are shown in Fig. 12. The $R2$ activation energy was slightly higher than the $R1$ activation energy. The lowest value of the activation energy, for both resistances, was observed at the 22% SOC, thus this indicates that the charge/discharge reaction easily occurs at this SOC.

The reaction resistance on the high frequency side corresponds to the anode and the reaction resistance on the low frequency side corresponds to the cathode as already mentioned; the activation energy of $R2$ at all the SOCs was bigger than the activation energy of $R1$. The values of the charge/discharge activation energy and deterioration are summarized in Table 3. The deterioration activation energy in comparison to the charge/discharge activation energy resulted was two times greater. The deterioration reaction and charge/discharge reaction are independent of each other. From the results in Table 3, it can be concluded that the cell degradation reactions are relatively difficult to occur when compared to the charge/discharge.

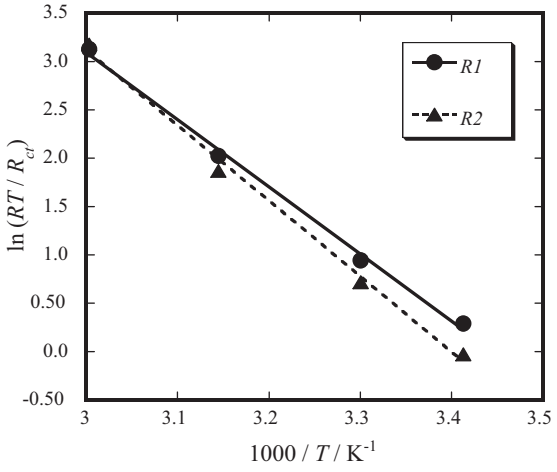


**Fig. 11.** Arrhenius plots of lithium-ion secondary cell at SOC = 87%. Data are taken from Table 2.

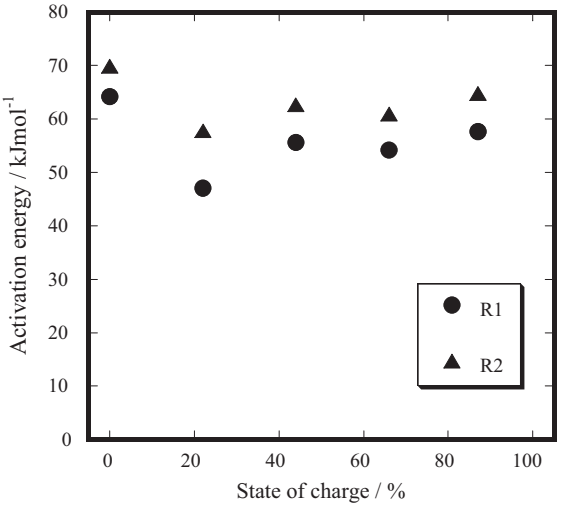


**Fig. 12.** Activation energies of lithium-ion secondary cells at various SOCs.

**Table 3**
Activation energy of charge–discharge and deterioration of lithium-ion secondary cells at various SOCs.

| SOC (%) | Activation energy (kJ mol$^{-1}$) | | |
|---|---|---|---|
| | Charge/discharge | | Deterioration |
| | $R1$ | $R2$ | |
| 0 | 64.2 | 69.9 | 145.9 |
| 22 | 47.1 | 57.8 | 134.6 |
| 44 | 55.6 | 62.7 | 111.6 |
| 66 | 54.2 | 60.9 | 101.8 |
| 87 | 57.6 | 64.8 | 133.1 |

## 4. Conclusions

Thermal runaway mapping experiments were carried out using commercial lithium-ion secondary cells. In order to obtain the deterioration activation energy in the non-self heating domain and the deterioration in the cell capacity, electrochemical measurements were recorded before and after running high temperature storage tests.

1. By mapping the thermal runaway, it was possible to clarify the SOC dependence on the temperature in the self-heating domain.
2. The lowest deterioration activation energy value and the lowest frequency factor value were obtained at the SOC of 66%. At the SOCs of 0 and 87%, the values of the deterioration activation energy and frequency factor tended to increase. This occurs when there is an unbalance of lithium-ions between the anode and cathode.
3. The charge/discharge activation energy was obtained from the recorded EIS measurements. The lowest charge/discharge activation energy value was found at the SOC of 22%.
4. The value of the resulting deterioration activation energy was double the charge/discharge activation energy value. This suggests that the deterioration reaction is difficult to produce compared to the charge/discharge reaction.

5. Since the thermal stability of lithium-ion secondary cells is one of the main issues for improvement them, the developed method is a very useful technique to evaluate the cells degradation under high temperature conditions.

## Acknowledgement

This work was supported by the "Li-EAD project" program from the New Energy and Technology Development Organization (NEDO), Japan.

## References

[1] A. Yoshino, Innovative Batteries Enhanced Power Supply for the Next Stage, NTS, Japan, 2006.
[2] H. Tamura, M. Morita, H. Ikeda, C. Iwakura, Function Chemistry of Electron and Ion, vol. 3, NTS, Japan, 2003, p. 442.
[3] J.S. Hong, H. Maleki, S. Al Hallaj, L. Ready, J.R. Selman, J. Electrochem. Soc. 145 (1998) 1489.
[4] J.S. Gnanaraj, E. Zinigrad, L. Asraf, H.E. Gottlieb, M. Sprecher, D. Aurbach, M. Schmidt, J. Power Sources 119–121 (2003) 794.
[5] Y. Wang, K. Zaghib, A. Guerfi, F.F.C. Bazito, R.M. Torresi, J.R. Dahn, Electrochim. Acta 52 (2007) 6346.
[6] I. Uchida, H. Ishikawa, M. Mohamedi, M. Umeda, J. Power Sources 119–121 (2003) 821.
[7] T.D. Hatchard, D.D. MacNeil, A. Basu, J.R. Dahn, J. Electrochem. Soc. 148 (2001) 755.
[8] J. Yamaki, Netsu Sokutei 30 (2003) 3.
[9] Y. Kita, T. Morikawa, Y. Inaba, T. Yao, Matsushita Tech. J. 52 (2006) 25.
[10] H. Ishikawa, M. Mohamedi, T. Itoh, I. Uchida, Electrochemistry 71 (2003) 1030.
[11] M.N. Richard, J.R. Dahn, J. Electrochem. Soc. 146 (1999) 2068.
[12] M.N. Richard, J.R. Dahn, J. Electrochem. Soc. 146 (1999) 2078.
[13] G. Venugopal, J. Power Sources 101 (2001) 231.
[14] X. Liu, H. Kusawaka, S. Kuwajima, J. Power Sources 97-98 (2001) 661.
[15] Y. Sone, H. Ooto, T. Eguro, T. Yoshida, M. Kubota, H. Yoshida, M. Yamamoto, S. Sakai, K. Ogawa, Y. Takeda, M. Uno, K. Hirose, M. Tajima, J. Kawaguchi, Electrochemistry 75 (2007) 950.
[16] M. Mohamedi, H. Ishikawa, I. Uchida, J. Appl. Electrochem. 34 (2004) 1103.
[17] K. Takeno, M. Ichimura, K. Takano, J. Yamaki, S. Okada, J. Power Sources 128 (2004) 67.
[18] H. Kondo, Y. Takeuchi, T. Sasaki, S. Kawauchi, Y. Itou, O. Hiruta, C. Okuda, M. Yonemura, T. Kamiyama, Y. Ukyo, J. Power Sources 174 (2007) 1131.
[19] B.A. Boukamp, Solid State Ionics 20 (1986) 31.
[20] A.J. Bard, L.R. Faulkner, Electrochemical Methods: Fundamentals and Applications, 2nd ed., J. Wiley & Sons, New York, 2000.
[21] P. Suresh, A.K. Shukla, N. Munichandraiah, J. Appl. Electrochem. 32 (2002) 267.